Scaling investigation of Fermi acceleration on a dissipative bouncer model

André Luis Prando Livorati, Denis Gouvêa Ladeira, and Edson D. Leonel
Departamento de Estatística, Matemática Aplicada e Computação, IGCE, Universidade Estadual Paulista, Avenida 24A, 1515 Bela Vista, CEP 13506-900, Rio Claro, São Paulo, Brazil
(Received 30 July 2008; published 11 November 2008)

The phenomenon of Fermi acceleration is addressed for the problem of a classical and dissipative bouncer model, using a scaling description. The dynamics of the model, in both the complete and simplified versions, is obtained by use of a two-dimensional nonlinear mapping. The dissipation is introduced using a restitution coefficient on the periodically moving wall. Using scaling arguments, we describe the behavior of the average chaotic velocities on the model both as a function of the number of collisions with the moving wall and as a function of the time. We consider variations of the two control parameters; therefore critical exponents are obtained. We show that the formalism can be used to describe the occurrence of a transition from limited to unlimited energy growth as the restitution coefficient approaches unity. The formalism can be used to characterize the same transition in two-dimensional time-varying billiard problems.

DOI: 10.1103/PhysRevE.78.056205 PACS number(s): 05.45.Pq, 05.45.Tp

I. INTRODUCTION

Fermi acceleration (FA) is a phenomenon in which a classical particle acquires unbounded energy from collisions with a massive moving wall [1,2]. Applications of FA have acquired a broad interest in different fields of physics including plasma physics [3], astrophysics [4,5], atomic physics [6], optics [7,8], and even the well-known time-dependent billiard problems [9,10]. The interesting question posed that should be answered is whether the FA results from the nonlinear dynamics itself, considering the complete absence of any imposed random motion. A one-dimensional model exhibiting such a phenomenon, which is modeled by a nonlinear mapping, is the bouncer model [11,12]. For two-dimensional time-dependent billiards (billiards with moving boundaries), the answer to this question is not unique; it depends on the kind of phase space for the corresponding static version of the problem. Therefore, as conjectured by Loskutov, Ryabov, and Akinshin [13] (this conjecture is known in the literature as the LRA conjecture), the regular dynamics for a fixed boundary implies a bound to the energy gained by the bouncing particle, but the chaotic dynamics of a billiard with a fixed boundary is a sufficient condition for FA in the system when a boundary perturbation is introduced. This conjecture was confirmed in different billiards [14–16]. FA was observed recently in a time-varying elliptical billiard [17]. The oval billiard, however, seems not to exhibit FA for the breathing case [18].

In this paper we reconsider the problem of a classical particle bouncing inelastically from a periodically time-varying wall in the presence of a constant gravitational field [19–27]. Our main goal is to understand and describe the phase transition present in this problem. The transition is from limited to unlimited energy growth when the damping coefficient (restitution coefficient) approaches unity. The problem is described using a two-dimensional nonlinear mapping for the variables velocity of the particle and time immediately after a collision with the moving wall. It is known that [28], for the nondissipative version of the problem and depending on both the control parameters and initial conditions, the particle can experience the phenomenon of FA. This phenomenon is observed in this problem due to the absence of invariant spanning curves in the phase space, which happens for specific conditions of the control parameters. As we shall show, when the collisions of the particle with the moving wall are innelastic (the particle experiences a fractional loss of energy upon colision with the moving wall), the phenomenon of unlimited energy growth is not observed [29]. This implies that there exists a restitution coefficient $\alpha \in (0,1]$. Then, for $\alpha=1$ all the collisions are elastic. We consider, however, the situation where $\alpha<1$. Moreover, for $\alpha<1$ the mapping possesses the property of shrinking the phase space area; thus, depending on the initial condition, a chaotic attractor can be observed. The principal focus of this paper is to describe the behavior of the average velocities of the chaotic attractor and use scaling arguments to characterize the transition from limited to unlimited energy growth for $\alpha \to 1$, when the dissipation disappears. Depending on the combination of the initial conditions and control parameters, the model can exhibit FA for $\alpha=1$. Thus the limit $\alpha \to 1$ characterizes this transition. We describe the model via a two-dimensional nonlinear mapping T that describes the system in terms of the variables velocity of the particle, v, and time t, i.e., $T(v_n,t_n)=(v_{n+1},t_{n+1})$, where n denotes the index of the nth collision with the wall. We consider in this paper both the complete [30,31] and the simplified versions of the model [32–34]. The complete model takes into account the full aspects of the dynamics in the sense that the motion of the platform leads to different kinds of collision, which we denote as (i) direct (or successive—those collisions that the particle has before leaving the region near the moving wall's allowed positions) and (ii) indirect collisions. The simplified model, however, consists of an approximation that disregards the displacement of the oscillating platform. However, it considers that the particle changes energy upon collision with the moving wall as if the wall were periodically moving. This approximation carries the advantage of avoiding the solution of transcendental equations, as they must be solved in the complete model [31]. It also retains the nonlinearity of the problem [35]. The study of both cases allows us to compare the critical exponents near

the transition and, as far as we know, has not been considered before using such an approach.

The paper is organized as follows. In Sec. II, we present all the details needed to construct a complete version of the model. We show some chaotic orbits and their positive Lyapunov exponent. We also discuss the behavior of the positive Lyapunov exponent as a function of the control parameters. Our numerical results obtained for the average velocity and deviation around the average velocity are presented in this section. We also present a simplified version of the problem and compare the results and critical exponents with those from the full model. In Sec. III the scaling description is made by using the averages obtained as a function of time. The critical exponents are obtained and a special discussion is made connecting the results found as a function of the collision number and time. Finally, in Sec. IV we summarize our results and present our concluding remarks.

II. THE MODEL, THE COMPLETE VERSION OF THE MAP, AND RESULTS FOR QUANTITIES AVERAGED OVER THE NUMBER OF COLLISIONS

The model under consideration consists of a classical particle of mass m which is suffering inelastic collisions with a periodically moving wall given by $y(t)=\varepsilon\cos(wt)$, where ε is the amplitude of oscillation and w is the angular frequency. Moreover, the particle is under the action of a constant gravitational field g. Thus the return mechanism of the particle for the next collision with the wall is due only to the gravitational field. We have assumed that the dissipation is introduced via a coefficient of restitution α such that $\alpha\in[0,1]$. The limit of $\alpha=1$ recovers the results for the nondissipative case while for $\alpha=0$ it is possible to observe the phenomenon of locking [22,23]. For the case where $\alpha<1$, the particle experiences a fractional loss of energy upon collisions with the moving wall. The description of the dynamics of the problem is made by use of a two-dimensional nonlinear mapping for the variables velocity of the particle v_n and time t_n immediately after the nth collision of the particle with the moving wall. The so-called complete version takes into account the movement of the moving wall. There are then two distinct kinds of collision that may arise from such a version, namely, (i) multiple collisions of the particle with the moving wall, which can happens before the particle leaves the collision zone (the collision zone is defined as the region $y\in[-\varepsilon,\varepsilon]$); or (ii) a single collision of the particle with the moving wall. In the case (ii) the particle leaves the collision zone after suffering a single collision with the moving wall. Before we write the equations of the mapping, we should point out that there are an excessive number of control parameters, four in total, namely, ε, g, w, and α. The dynamics, however, does not depend on all of them, and we can define the dimensionless variables $V_n=v_nw/g$, $\epsilon=\varepsilon w^2/g$, and measure the time as $\varphi_n=wt_n$. Considering this set of new variables and assuming that the initial conditions for the dynamics are $V_n>0$, $\varphi_n\in[0,2\pi]$, and the position of the particle at the instant φ_n is $y_p(\varphi_n)=\epsilon\cos(\varphi_n)$, we obtain the mapping written as

$$T:\begin{cases} V_{n+1}=-\alpha(V_n^*-\phi_c)-(1+\alpha)\epsilon\sin(\phi_{n+1}), \\ \phi_{n+1}=(\phi_n+\Delta T_n)\mod(2\pi), \end{cases} \tag{1}$$

where the expressions for V_n^* and ΔT_n depend on what kind of collision happens. For the case (i), i.e., multiple collisions, the corresponding expressions are $V_n^*=V_n$ and $\Delta T_n=\varphi_c$. The term φ_c is obtained from the condition that matches the positions for the particle and the moving wall. This condition gives rise to the transcendental equation

$$G(\phi_c)=\epsilon\cos(\phi_n+\phi_c)-\epsilon\cos(\phi_n)-V_n\phi_c+\frac{1}{2}\phi_c^2. \tag{2}$$

If the particle leaves the collision zone, then case (ii) applies, and the corresponding expressions are $V_n^*=-\sqrt{V_n^2+2\epsilon[\cos(\varphi_n)-1]}$ and $\Delta T_n=\varphi_u+\varphi_d+\varphi_c$, with $\varphi_u=V_n$ denoting the time spent by the particle moving in the upward direction until it reaches the null velocity, and $\varphi_d=\sqrt{V_n^2+2\epsilon[\cos(\varphi_n)-1]}$ corresponds to the time that the particle takes to move from the place where it had zero velocity to the entrance of the collision zone. Finally, the term φ_c has to be found numerically from the equation $F(\varphi_c)=0$, where

$$F(\phi_c)=\epsilon\cos(\phi_n+\phi_u+\phi_d+\phi_c)-\epsilon-V_n^*\phi_c+\frac{1}{2}\phi_c^2. \tag{3}$$

After some straightforward algebra, it is easy to show that the mapping (1) shrinks the phase space measure, since the determinant of the Jacobian matrix is given by

$$\mathrm{Det}J=\alpha^2\left(\frac{V_n+\epsilon\sin(\phi_n)}{V_{n+1}+\epsilon\sin(\phi_{n+1})}\right). \tag{4}$$

In order to see the behavior that can emanate from iteration of the mapping (1), Fig. 1 shows the behavior of chaotic orbits for four different sets of control parameters. In Fig. 1(a) $\alpha=0.99$ and $\epsilon=10$, while in Fig. 1(b) $\alpha=0.999$ and $\epsilon=10$. For Fig. 1(c) $\alpha=0.99$ and $\epsilon=100$ and finally for Fig. 1(d) $\alpha=0.999$ and $\epsilon=1000$. Each initial condition was iterated up to 10^7 collisions with the moving wall. We can see that, even for a long evolution of 10^7 collisions, the orbits do not seem to show unlimited energy growth. To check whether the orbits shown in Fig. 1 are chaotic, the Lyapunov exponent must be evaluated. It is known that the Lyapunov exponent is a common tool used to characterize the sensitivity to the initial conditions. The procedure consisits in evolving the system over a long time from two slightly different initial conditions. If the two trajectories diverge exponentially in time the orbit is called chaotic and the Lyapunov exponent obtained is positive. Let us describe briefly the procedure used to obtain the Lyapunov exponents numerically. They are defined [36] as

$$\lambda_j=\lim_{n\to\infty}\ln|\Lambda_j|,\quad j=1,2,$$

where Λ_j are the eigenvalues of $M=\Pi_{k=1}^{n}J_k(V_k,\varphi_k)$ and J_k is the Jacobian matrix evaluated along the orbit (V_k,φ_k).

Figure 2 shows the convergence of the positive Lyapunov exponents as a function of the number of collisions with the moving wall for the complete version of the dissipative bouncer model. We see that, when five different initial con-

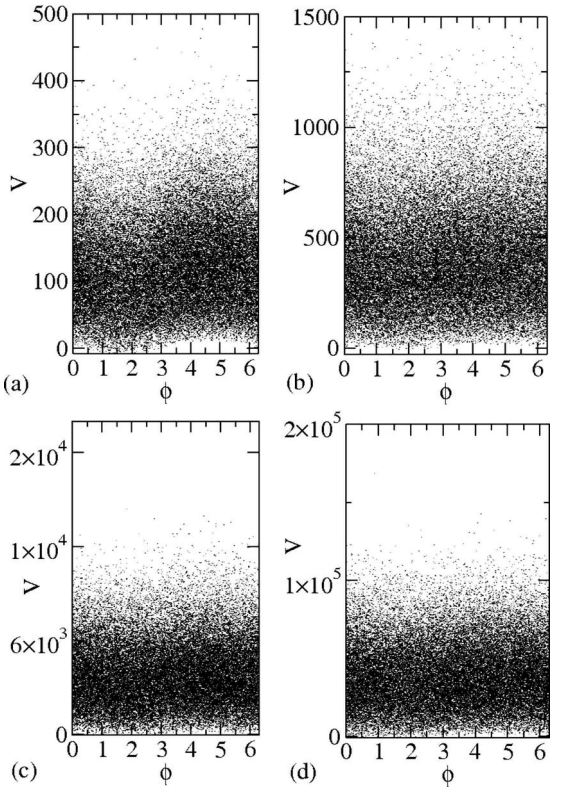

FIG. 1. Chaotic orbits for a full version of the dissipative bouncer model. The control parameters used in the construction of the figures were (a) $\alpha=0.99$ and $\epsilon=10$; (b) $\alpha=0.999$ and $\epsilon=10$; (c) $\alpha=0.99$ and $\epsilon=100$; (d) $\alpha=0.999$ and $\epsilon=1000$.

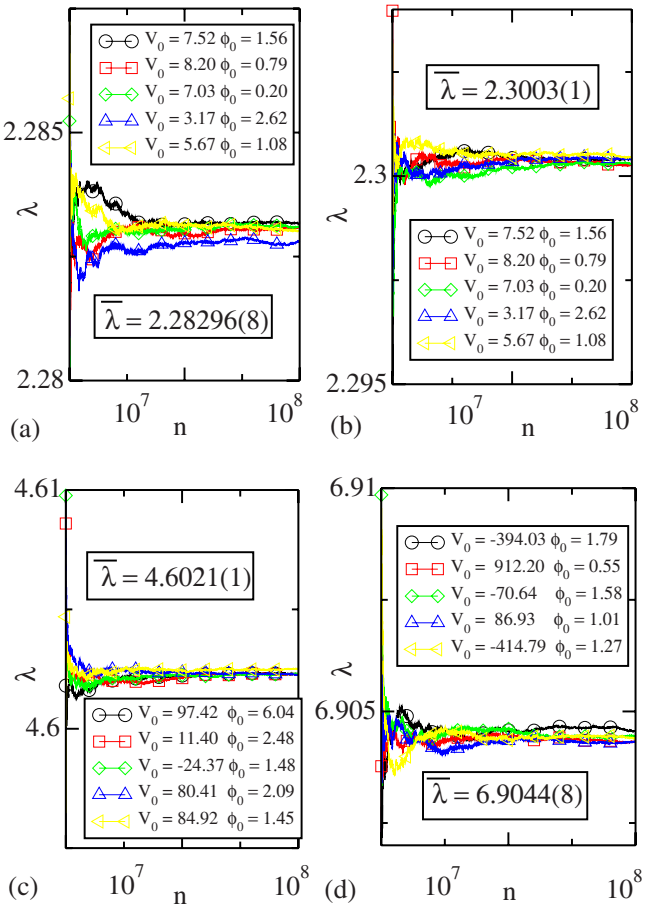

FIG. 2. (Color online) Convergence for the positive Lyapunov exponent. The control parameters used were (a) $\alpha=0.99$ and $\epsilon=10$; (b) $\alpha=0.999$ and $\epsilon=10$; (c) $\alpha=0.999$ and $\epsilon=100$; (d) $\alpha=0.999$ and $\epsilon=1000$.

ditions are evolved in time, all of them converge to a constant value for large n. This convergence allows us to obtain the average value for the positive Lyapunov exponent over the chaotic attractor. The control parameters used in the construction of the Fig. 2 were (a) $\alpha=0.99$ and $\epsilon=10$; (b) $\alpha=0.999$ and $\epsilon=10$; (c) $\alpha=0.999$ and $\epsilon=100$; (d) $\alpha=0.999$ and $\epsilon=1000$. The corresponding medium values are shown in the figure.

Let us now discuss the behavior of the positive Lyapunov exponent as a function of the control parameters ϵ and α. Figure 3 shows the behavior of (a) $\bar{\lambda}$ vs $(1-\alpha)$ and (b) $\bar{\lambda}$ vs ϵ. We can see in Fig. 3(a) that the positive Lyapunov exponent is almost constant over the two initial decades in the log-linear graph and then decreases for $(1-\alpha)\approx 10^{-3}$. Thus an exponential fit give us that $\bar{\lambda}=2.302\,50(2)\exp[-0.861(5)(1-\alpha)]$. On the other hand, the positive Lyapunov exponent is more sensitive to the dependence on ϵ, as shown in Fig. 3(b). The log-linear graph shows an increase in $\bar{\lambda}$ as ϵ increases. Such behavior is better fitted by a logarithmic function of the type $\bar{\lambda}=-0.001\,71(6)+0.999\,76(1)\ln(\epsilon)$.

We now concentrate on obtaining some statistical properties of the chaotic time series. We shall investigate the behavior of the deviation of the average velocity for chaotic orbits. The deviation of the average velocity therefore exhibits similar properties as the average velocity [29,37]. Before we define the deviation of the average velocity properly, it is important first to know the average velocity, which is given by

$$\bar{V}(n,\epsilon,\alpha)=\frac{1}{n}\sum_{i=0}^{n}V_i. \tag{5}$$

Then, the deviation around the average velocity is defined as

$$\omega(n,\epsilon,\alpha)=\frac{1}{M}\sum_{i=1}^{M}\sqrt{\bar{V^2}_i(n,\epsilon,\alpha)-\bar{V}_i^2(n,\epsilon,\alpha)}. \tag{6}$$

The behavior of ω as a function of n is shown in Fig. 4. To construct the curves shown in Fig. 4 we have evolved an ensemble of 10^3 different initial phases for the same initial velocity $V_0=\epsilon$. The situation where different initial velocities are considered can be found, for a version of the Fermi-Ulam model [38], in [30,32]. Each initial condition was iterated up to 10^7 collisions with the moving wall. One can see that the curve starts growing for a small number of collisions and then suddenly it bends toward a regime of convergence marked by a constant plateau. The changeover from growth to saturation is characterized by a typical number of collisions, indicated in the figure as n_x. This kind of behavior is observed for different combinations of control parameters.

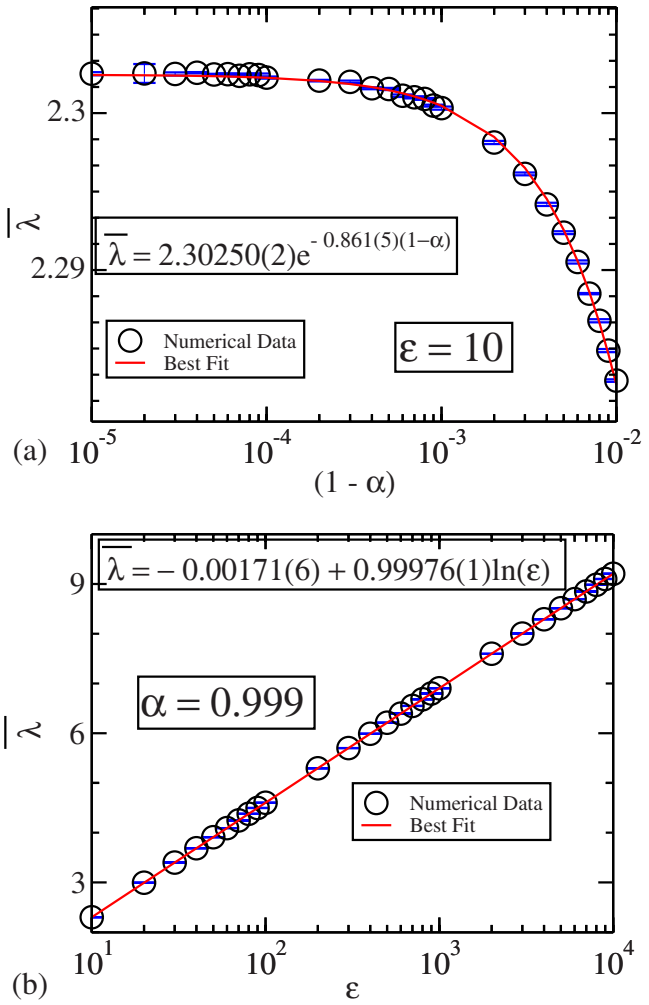

FIG. 3. (Color online) Plot of the averaged positive Lyapunov exponent as a function of (a) $(1-\alpha)$ and (b) ϵ.

However, those curves constructed for different values of ϵ start growing at different positions, thus indicating that n is not a good variable. However, if we apply the transformation $n \to n\epsilon^2$ all curves start growing together, as shown in Fig. 4(b).

The behavior of the curves shown in Fig. 4(b) motivates us to suppose the following scaling hypotheses.

(1) For a small number of collisions with the moving wall, the behavior of ω can be described by a power law of the type

$$\omega \propto (n\epsilon^2)^{\beta}, \tag{7}$$

where β is the critical exponent. Applying a power law fitting in Fig. 4(b), we obtain $\beta = 0.479(8) \cong 0.5$.

(2) For a sufficient long n, the saturation of ω (we denote it as ω_{sat}) is given by

$$\omega_{\text{sat}} \propto (1-\alpha)^{\gamma_1} \epsilon^{\gamma_2}, \tag{8}$$

where both γ_1 and γ_2 are also critical exponents.

(3) Finally, the number of collisions that characterizes the changeover from growth to the saturation regime is given by

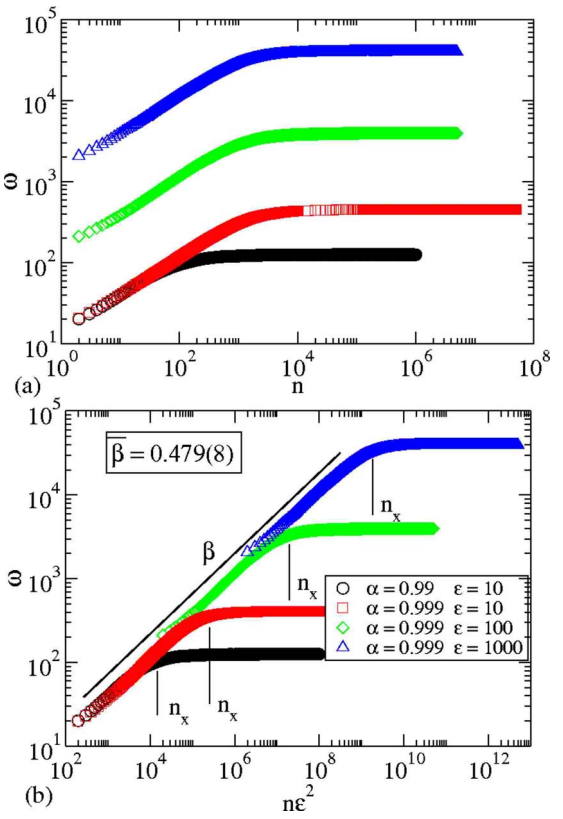

FIG. 4. (Color online) (a) Plot of ω as a function of n. (b) The same plot shown in (a) after the transformation $n \to n\epsilon^2$. The control parameters used in the construction of these curves are shown in the figure.

$$n_x \epsilon^2 \propto (1-\alpha)^{z_1} \epsilon^{z_2}, \tag{9}$$

where z_1 and z_2 are called dynamical exponents.

Instead of considering the variable α, we do better to choose to describe the average properties as functions of $1-\alpha$. This transformation brings the criticality to $(1-\alpha) \to 0$.

To obtain the critical exponents γ_1 and γ_2, we must evolve a simulation for a very long n. Thus, using extrapolation we can obtain the values of ω_{sat} as functions of $(1-\alpha)$ and ϵ. The exponents z_1 and z_2 are obtained via a crossing of the values obtained for the saturation and the initial growth regime. The behavior of ω_{sat} and n_x as functions of both $(1-\alpha)$ and ϵ is shown in Fig. 5. One of the most important results of this paper is evident from a careful investigation of Eqs. (8) and (9) for the critical exponents $\gamma_1 \cong -0.5$ and $z_1 \cong -1$. Clearly, both Eqs. (8) and (9) diverge for the limit of $\alpha \to 1$. In particular, Eq. (8) recovers the phenomenon of Fermi acceleration for the limit of $\alpha \to 1$.

Considering these scaling hypotheses, we can now describe ω in terms of a scaling function of the type

$$\omega((1-\alpha)\epsilon^y, n\epsilon^2) = l\omega(l^a(1-\alpha)\epsilon^y, l^b(n\epsilon^2)), \tag{10}$$

where l is the scaling factor and a and b are scaling exponents. Choosing $l = (n\epsilon^2)^{-1/b}$, we have,

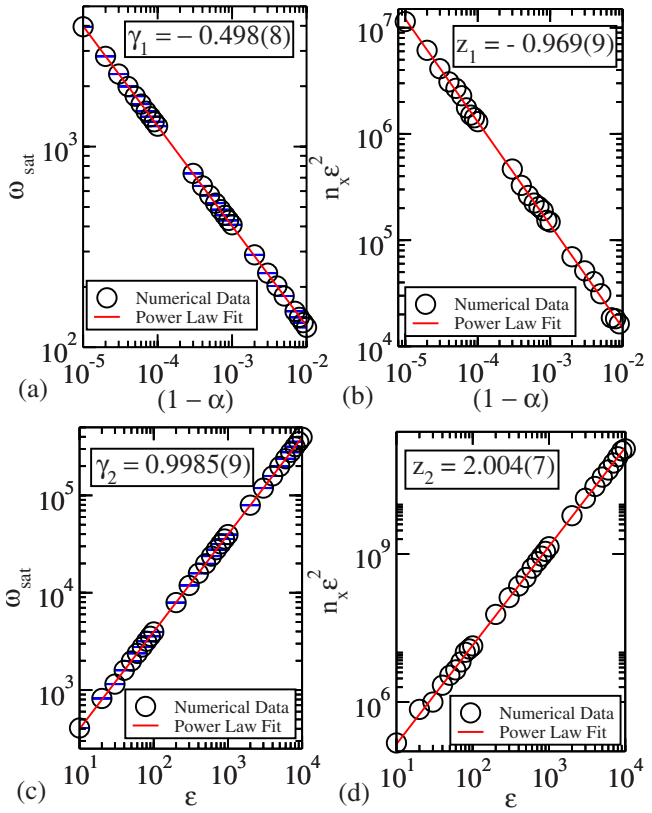

FIG. 5. (Color online) Behavior of (a) ω_{sat} vs $(1-\alpha)$, (b) n_x vs $(1-\alpha)$, (c) ω_{sat} vs ϵ, and (d) $n_x\epsilon^2$ vs ϵ.

$$\omega(\epsilon^y(1-\alpha), n\epsilon^2) = (n\epsilon^2)^{-1/b}\omega_1((n\epsilon^2)^{-a/b}(1-\alpha)\epsilon^y), \tag{11}$$

where we assume that ω_1 is constant for $n_x \gg n$. From Eq. (11) we obtain the following expression for the crossover number:

$$n_x\epsilon^2 \propto [(1-\alpha)\epsilon^y]^{b/a}. \tag{12}$$

Using the above relation and Eq. (9), we obtain

$$\frac{b}{a} = z_1, \quad \frac{yb}{a} = z_2. \tag{13}$$

Thus the numerical value for y is

$$y = \frac{z_2}{z_1} = -2.07 \pm 0.01. \tag{14}$$

Now choosing, $l=[(1-\alpha)\epsilon^y]^{-1/a}$, we have

$$\omega(\epsilon^y(1-\alpha), n\epsilon^2) = [(1-\alpha)\epsilon^y]^{-1/a}\omega_2((1-\alpha)\epsilon^{y-b/a}(n\epsilon^2)), \tag{15}$$

where we assume ω_2 as constant for $n_x \ll n$. From Eq. (15) we obtain the expression for ω_{sat},

$$\omega_{\text{sat}} \propto [(1-\alpha)\epsilon^y]^{-1/a}. \tag{16}$$

From the above equation and Eq. (8), we have

$$-\frac{1}{a} = \gamma_1, \quad -\frac{y}{a} = \gamma_2. \tag{17}$$

These expressions give us the numerical values of the exponents a and y as

$$a = -\frac{1}{\gamma_1} = 2.00 \pm 0.03, \tag{18}$$

$$y = \frac{\gamma_2}{\gamma_1} = -2.00 \pm 0.03. \tag{19}$$

After this discussion, we can see that both Eq. (14) and Eq. (19) give $y \cong -2$. Considering the limit $n\epsilon^2 \ll n_x\epsilon^2$, we can rewrite Eq. (15) as

$$\omega(\epsilon^y(1-\alpha), n\epsilon^2) = [(1-\alpha)\epsilon^y]^{-1/a}\{[(1-\alpha)\epsilon^{y-b/a}(n\epsilon^2)]\}^{\beta}. \tag{20}$$

Thus, for the regime of growth we have

$$-\frac{y}{a} - \frac{\beta by}{a} = -\frac{1}{a} - \frac{\beta b}{a} = 0. \tag{21}$$

Considering Eq. (21) and Eqs. (13) and (20), we obtain

$$b = -\frac{1}{\beta} = -2.08 \pm 0.03, \tag{22}$$

$$b = -\frac{z_2}{\gamma_2} = -2.007 \pm 0.005. \tag{23}$$

We therefore obtain that $b \approx -2$. Considering Eqs. (13), (20), and (21), we have the numerical value for a as

$$a = \frac{y}{\beta z_2} = \frac{1}{\beta z_1} \approx 2. \tag{24}$$

To check whether these initial suppositions are correct, let us now obtain a universal plot of different curves generated from different control parameters. The behavior of ω as a function of n for different values of control parameters is shown in Fig. 6. One can see that, after reescaling the coordinate axes according to the critical exponents obtained above, all curves generate a single and universal plot.

A. A simplified model and numerical results for averages over the number of collisions

Let us discuss in this section a simplified version of the problem. The simplification consists basically in considering that, when the particle hits the wall, it suffers an exchange of energy and momentum as if the wall were moving [33,35]. This is a common approximation used to speed up the numerical simulation, since no transcendental equations must be solved as they must be in the complete version. The simplified version also retains the nonlinearity of the problem. The mapping is then written as

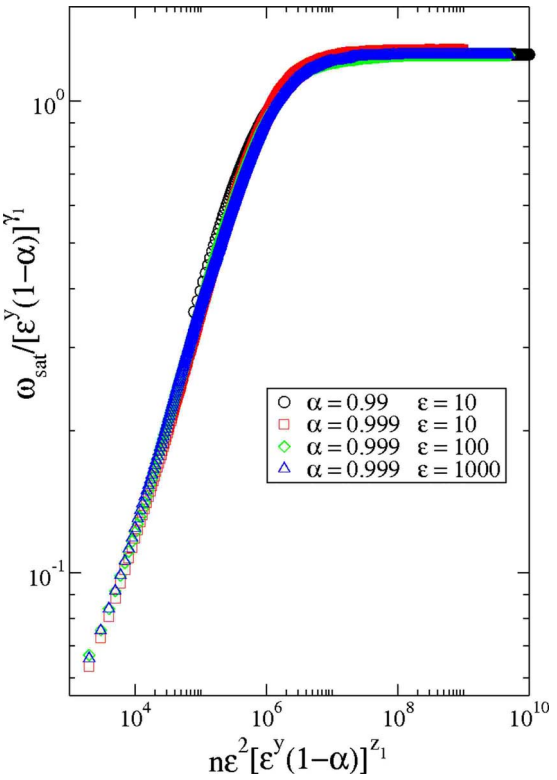

FIG. 6. (Color online) Universal plot for different curves of ω.

$$T:\begin{cases} V_{n+1} = |\alpha V_n - (1+\alpha)\epsilon \sin(\phi_{n+1})|, \\ \phi_{n+1} = [\phi_n + 2V_n] \mod(2\pi). \end{cases} \tag{25}$$

This mapping also shrinks the area on the phase space for $\alpha<1$ since Det $J=\alpha\,\mathrm{sgn}[\alpha V_n-(1+\alpha)\epsilon\sin(\varphi_{n+1})]$, where the function $\mathrm{sgn}(u)=1$ if $u>0$ and $\mathrm{sign}(u)=-1$ if $u<0$, and J is the Jacobian matrix. It is important to say that in the simplified model negative velocities of the particle after a collision with the wall are forbidden, because such velocities would be equivalent to the particle moving beyond the wall. In order to avoid such problems, if after the collision with the wall the particle acquires a negative velocity, we inject it back with the same modulus of velocity. This procedure is effected by use of a modulus function. Note that the velocity of the particle is reversed by the modulus function only if, after the collision, the particle remains traveling in the negative direction. The modulus function has no effect on the motion of the particle if the particle moves in the positive direction after the collision.

Chaotic orbits are also present in this version of the model. The convergence of the Lyapunov exponents is observed by using the same algorithm as used for the complete version. Thus, we can obtain the behavior of the positive Lyapunov exponent as a function of ϵ and α. In Fig. 7 is shown the behavior of $\bar{\lambda}$ vs ϵ and $\bar{\lambda}$ vs $(1-\alpha)$. The functions that fit the numerical data are the same as those obtained for the complete model. However, the coefficients are a little different. Their corresponding fits are shown in the figure.

Let us now discuss the differences obtained for the positive Lyapunov exponents based on the behavior of the histograms of frequency concerning the chaotic attractors for both the complete and simplified versions of the model. Such an analysis is important since we have differences in the asymptotic values for the positive Lyapunov exponents. It is shown in Fig. 8 the behavior of the histogram of frequency for the (a) simplified and (b) complete versions of the model. We can clearly see that the two are rather different from each other in the low- and average-energy regimes and quite similar for the high-energy regime, where they experience a decay. The difference in the low-energy regime is basically due to the reinjection of the particle that occurs in the simplified version of the model. This reinjection is caused by the modulus function. In the simplified model, the frequency is slightly sparse in the regime of low energy, mainly because of the action of the modulus function, and then it converges to a thin curve which experiences a decay for the regime of high energy. The behavior of the histogram of frequency for the complete model is different in the regime of low energy. We can see that the frequency at low energy is low but very well defined. Then it rises rapidly, passing by a maximum value, and experiences a decay for the regime of high energy. Thus the complete model has a *preference* for average velocities. This kind of behavior is the main explanation for the differences in values obtained for the positive Lyapunov exponents when we compare the simplified and complete versions of the model.

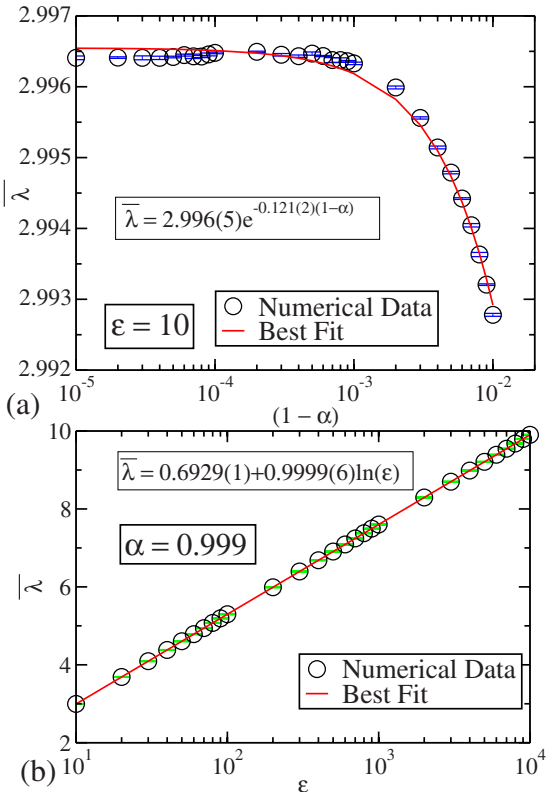

FIG. 7. (Color online) Behavior of $\bar{\lambda}$ vs ϵ and $\bar{\lambda}$ vs $(1-\alpha)$.

The behavior of the histogram of frequency for the complete model seems to be universal since it has the same general form for different control parameters. Figure 9(a) illustrates the behavior of the histogram of frequency for different control parameters, as labeled in the figure. We can

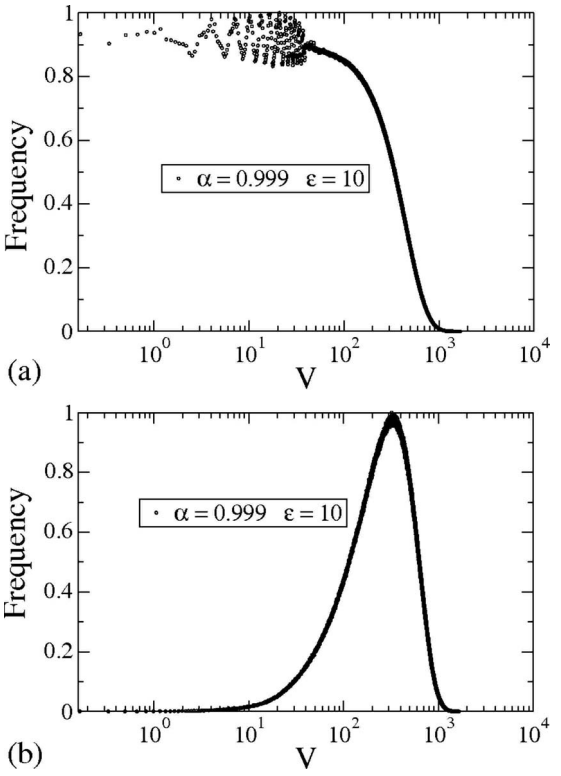

FIG. 8. Frequency histograms, for the variable velocity, of chaotic attractors for (a) simplified and (b) complete versions of the model. The control parameters used were $\alpha=0.999$ and $\epsilon=10$.

see that the peaks of the histograms depend on the control parameters. We suppose that the velocity of the peaks can be described as

$$V_p \propto \epsilon^{\mu}(1-\alpha)^{\delta}, \tag{26}$$

where μ and δ are exponents to be obtained. Considering different combinations of control parameters, we obtain the values of the velocity in the peak, which we denote as V_p, by fitting a polynomial of second order around the region of peak. Thus, by finding the value where this polynomial assumes a maximum, we easily obtain the peak value. This value is then plotted against the control parameters, as shown in Fig. 10. Thus, after fitting power laws, we obtain that $\mu=-0.487(5)\cong-0.5$ and $\delta=1.00(6)\cong 1$. With these values, we can then apply a reescaling in the velocity axis and collapse all the curves onto a single and universal curve, as shown in Fig. 9(b).

B. Scaling as function of the number of collisions

As discussed in the previous section, the simplified version of the model also allows us to describe their statistical properties by using scaling arguments. The results as a function of the damping coefficient are already known in the literature (see Ref. [37]), but not the description as a function of the parameter ϵ, to our knowledge. After doing extensive simulation to obtain the critical exponents, we found that their values are rather similar, considering the margin of uncertainty. The critical exponents we found for the simplified

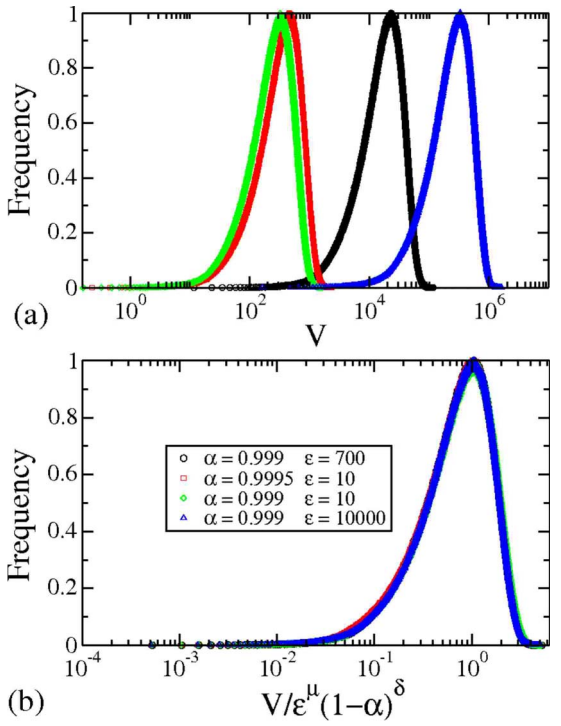

FIG. 9. (Color online) (a) Frequency histograms, for the variable velocity, regarding chaotic attractors for the complete version of the model. (b) Their collapse onto a single and universal curve.

version are $\gamma_1=-0.4983(9)$, $z_1=-0.9818(1)$, $\gamma_2=0.9983(1)$, and $z_2=1.9940(3)$. Therefore, the collapse of all the curves of the deviation of the average velocity is pretty similar to the one shown in Fig. 6.

III. ANALYSIS OF THE SIMPLIFIED VERSION ON VARIABLE TIME

In this section we describe the scaling properties of the bouncer model when average properties of the system are evaluated over time. The main interest in such an analysis lies in the fact that the collision number is not necessarily

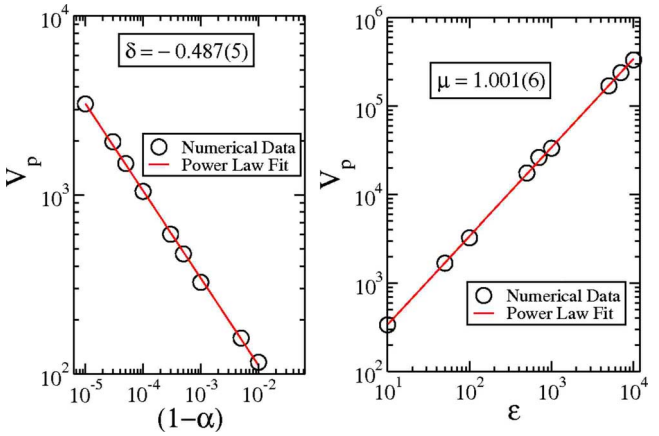

FIG. 10. (Color online) Behavior of V_p as a function of the control parameters.

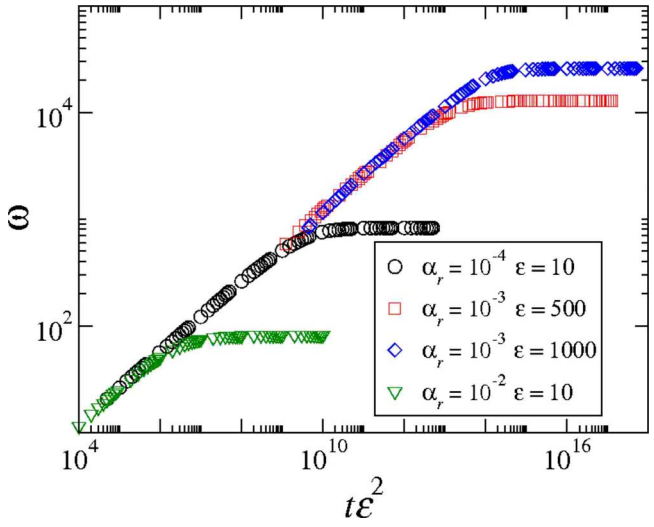

FIG. 11. (Color online) Log-log plot of ω as a function of $t\varepsilon^2$ for different values of α_r and ε.

proportional to time, as discussed by Lichtenberg and Lieberman [39].

A. Scaling of the deviation of the velocity

Before we present the scaling description let us introduce the average quantities that we are going to deal with. Regarding at first the orbit of an initial condition i, we evaluate the average velocity using the expression

$$\overline{V}_i(\varepsilon,\alpha,t) = \frac{1}{t}\int_0^t V_i(\varepsilon,\alpha,\tau)d\tau. \tag{27}$$

Now we regard an ensemble of M chaotic trajectories and we obtain the average value of the deviation of the velocity,

$$\omega(\varepsilon,\alpha,t) = \frac{1}{M}\sum_{i=1}^{M}\sqrt{\overline{V}_i^2(\varepsilon,\alpha,t) - \overline{V}_i^2(\varepsilon,\alpha,t)}. \tag{28}$$

The scaling description is more straightforward when we replace t by the new variable $t\varepsilon^2$. Figure 11 shows the ω curves for different values of the control parameters $\alpha_r = 1-\alpha$ and ε, as labeled in the figure.

We observe in Fig. 11 that the initial growth of the ω curves depends only on $t\varepsilon^2$ according to the expression

$$\omega \propto (t\varepsilon^2)^{\beta}, \tag{29}$$

where β is the growth exponent. Performing power law fittings to the numerical data in the growth regime, we obtain the average value $\beta = 0.334 \pm 0.008 (\approx 1/3)$.

In the limit of large values of $t\varepsilon^2$, when the deviation of the velocity reaches constant values, ω depends on ε and α_r. Thus we describe the saturation regime of ω as

$$\omega_{\text{sat}} \propto \varepsilon^{\gamma_1}\alpha_r^{\gamma_2}, \tag{30}$$

where γ_1 and γ_2 are the saturation exponents. We obtain the exponent γ_1 by plotting ω_{sat} versus ε with a fixed value of α_r and, similarly, we obtain γ_2 by fitting the numerical data in a plot of ω_{sat} as a function of α_r for a fixed value of ε. Figures 12(a) and 12(b) illustrate the procedure, which furnishes $\gamma_1 = 0.99 \pm 0.01$ and $\gamma_2 = -0.510 \pm 0.001$. Because γ_2 is negative we observe that ω diverges in the limit $\alpha_r \to 0$, an expected result.

The change from growth to the saturation regime defines the variable $t_z\varepsilon^2$. This crossover is a function of ε and α_r according to

$$t_z\varepsilon^2 \propto \varepsilon^{z_1}\alpha_r^{z_2}, \tag{31}$$

where z_1 and z_2 are the dynamical exponents. We obtain these exponents by fitting the numerical data $t_z\varepsilon^2$ versus ε and $t_z\varepsilon^2$ versus α_r, as we present, respectively, in Figs. 12(c) and 12(d). The procedure furnishes $z_1 = 2.98 \pm 0.02$ and $z_2 = -1.49 \pm 0.01$. Because z_2 is negative we observe that the time until the saturation regime diverges for $\alpha_r \to 0$. This result indicates that ω diverges in the elastic collision limit.

In Fig. 11 we observe that ω depends on ε, α_r, and $t\varepsilon^2$. However, the appropriate scaling variables of the average quantity ω are $\varepsilon^y\alpha_r$ and $t\varepsilon^2$, where y is an exponent related to the critical exponents. Near the transition from limited to unlimited energy growth, $\alpha_r \approx 0$, we suppose that ω obeys the homogeneous equation

$$\omega(\varepsilon^y\alpha_r, t\varepsilon^2) = l\omega(l^a\varepsilon^y\alpha_r, l^b t\varepsilon^2). \tag{32}$$

Choosing $l = (\varepsilon^y\alpha_r)^{-1/a}$, we have that the crossover is described by $t_z\varepsilon^2 \propto (\varepsilon^y\alpha_r)^{b/a}$. This relation and Eq. (31) furnish $z_1 = yb/a$ and $z_2 = b/a$. These relations give that the exponent y of Eq. (32) obeys the expression $y = z_1/z_2 = -2.00 \pm 0.03$.

In the limit of large values of $t\varepsilon^2$ we have that ω does not depend on time. Thus Eqs. (32) and (30) furnish the relations $\gamma_1 = -y/a$ and $\gamma_2 = -1/a$. These expressions give us $a = -1/\gamma_2 = 1.961 \pm 0.004$ and $y = \gamma_1/\gamma_2 = -1.94 \pm 0.02$. Regarding the uncertainties, we observe that $y = z_1/z_2 = \gamma_1/\gamma_2 \approx -2$.

Regarding the limit $t\varepsilon^2 \ll t_z\varepsilon^2$, we have for the growth regime that the exponents satisfy the relation $-y/a - \beta by/a = -1/a - \beta b/a = 0$. We combine this result with the relations obtained above for the exponents z_1, z_2, γ_1, and γ_2 and we obtain that $\gamma_1 - \beta z_1 = 0$ and $\gamma_2 - \beta z_2 = 0$. Moreover, we have that the scaling exponent b satisfies the relation $b = -1/\beta = -z_1/\gamma_1 \approx -3$. Furthermore, we find that $a = -1/\gamma_2 = -1/(\beta z_2) = -y/\gamma_1 \approx 2$.

With the scaling exponents a and b above we obtain the universal behavior of the curves of ω. Figure 13 shows the collapse of the ω curves onto a single and universal curve. This result confirms that the transition from unlimited to limited growth of ω presents scaling behavior, as initially proposed in Eq. (32).

As showed in Ref. [34], the average energy of the simplified version of the Fermi-Ulam model decays in the limit of large values of time. This result contrasts with the saturation of ω in the limit of large times, as we see in Fig. 11. Although the Fermi-Ulam and bouncer models are similar, the mathematical description of these systems is different. In the Fermi-Ulam model the time between two collisions is $\Delta t = 2/V$, while in the bouncer model $\Delta t = 2V$. Thus these systems present different behaviors for small and large values of the velocity and different behaviors for large values of time.

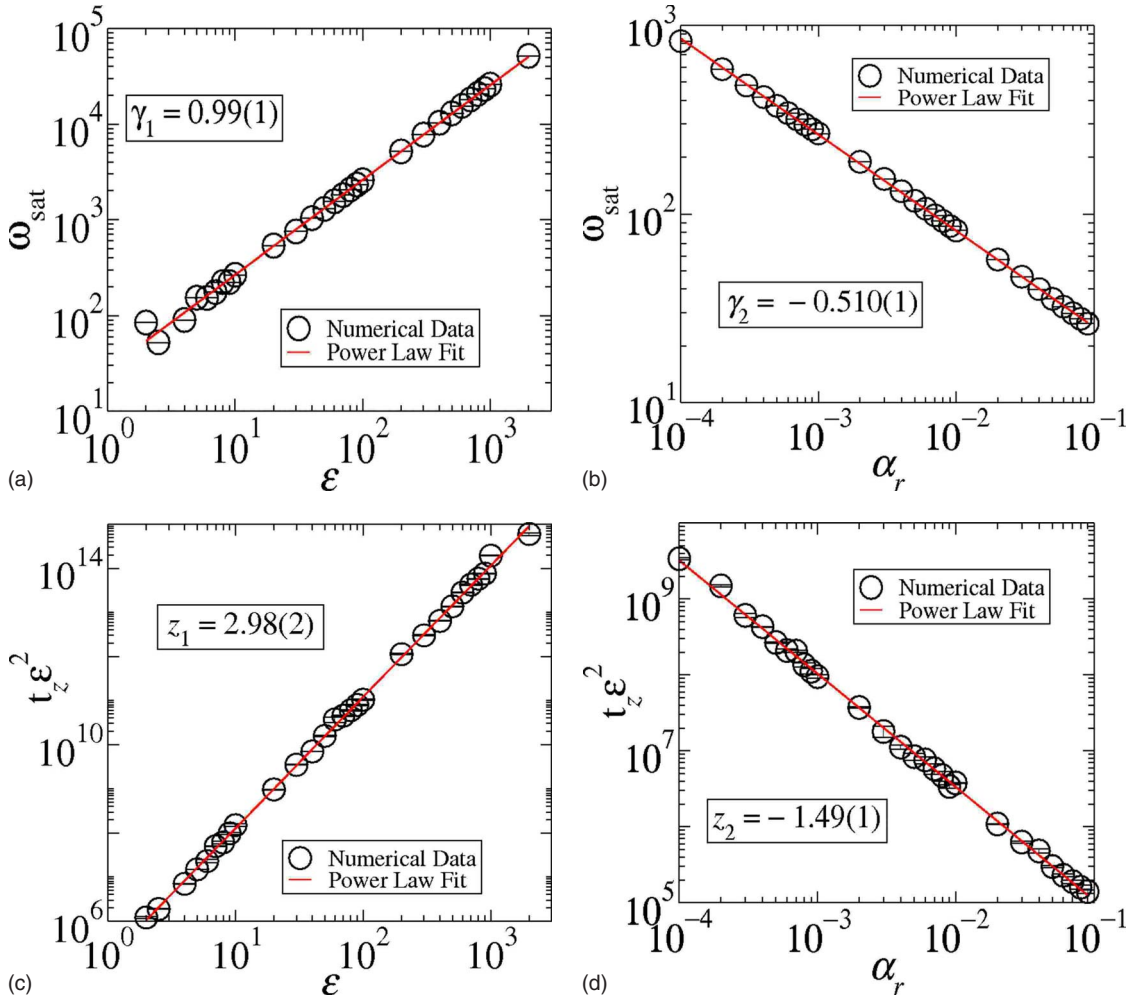

FIG. 12. (Color online) (a) Saturation values of deviation of the velocity as function of ε. A power law fit gives $\gamma_1=0.99(1)$. (b) shows the least-squares fit to the numerical values of ω_{sat} as a function of the parameter α_r. The procedure furnishes $\gamma_2=-0.510(1)$. (c) and (d) show, respectively, the crossover value $t_z\varepsilon^2$ as a function of ε and α_r. The corresponding fits furnish $z_1=2.98(2)$ and $z_2=-1.49(1)$.

B. Scaling of the average collision number

We define $N_i(t)$ as the collision number between the particle and the moving wall until the time t. Thus, regarding an ensemble of M different initial conditions, we define the average collision number as

$$N(t) = \frac{1}{M}\sum_{i=1}^{M} N_i(t). \tag{33}$$

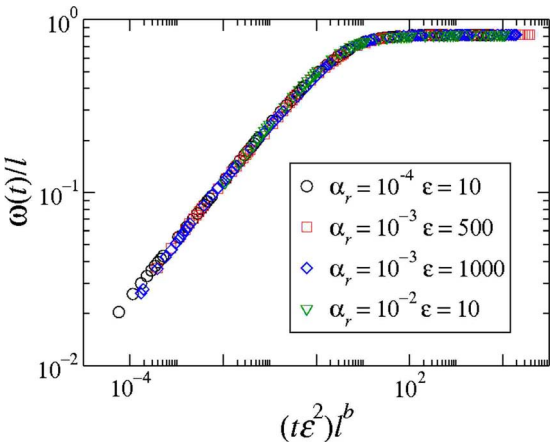

FIG. 13. (Color online) Collapse of the ω curves into a single and universal curve.

Figure 14 illustrates some curves of the average collision number as a function of $t\varepsilon^2$. These figures illustrate the behavior of N for different values of α_r and ε.

We observe in Fig. 14 that the N curves present two growth regimes. The initial growth regime does not depend on α_r. Thus we describe this initial regime as

$$N \propto (t\varepsilon^2)^{\xi_1}\varepsilon^{\eta_1}. \tag{34}$$

We obtained the growth exponent ξ_1 from power law fittings to the numerical data for different collision number curves. Thus we obtained the average value $\xi_1=0.69\pm0.02$. Figure 15(a) shows the numerical data in an $N/(t\varepsilon^2)^{\xi_1}$ vs ε plot. The best fit to these data furnishes $\eta_1=-2.12\pm0.01$.

For large values of $t\varepsilon^2$ we describe the average collision number as

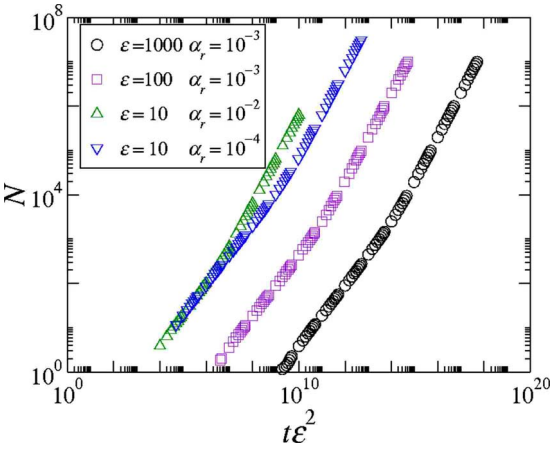

FIG. 14. (Color online) Average collision number curves as functions of $t\varepsilon^2$ for different values of ε and α_r.

$$N \propto (t\varepsilon^2)^{\xi_2}\varepsilon^{\eta_2}\alpha_r^{\zeta}. \tag{35}$$

We obtained the growth exponent ξ_2 for different curves and the average value is $\xi_2=0.9999\pm0.0002$. With a fixed value of α_r we performed a power law fit to the numerical data in a plot of $N/(t\varepsilon^2)^{\xi_2}$ vs ε. The procedure furnishes $\eta_2=-2.97\pm0.01$, as presented in Fig. 15(b). In the large-$t\varepsilon^2$ limit we obtain the exponent ζ from an $N/(t\varepsilon^2)^{\xi_2}$ vs α_r plot with a fixed value of ε. Figure 15(c) illustrates the procedure that furnishes $\zeta=0.492\pm0.005$.

The change between the growth regimes defines the quantity $t_z\varepsilon^2$. We describe this crossover as

$$t_z\varepsilon^2 \propto \varepsilon^{z_1}\alpha_r^{z_2}. \tag{36}$$

The values of the dynamical exponents are $z_1\approx3$ and $z_2\approx-3/2$, essentially the same as those that we obtained in the previous section, when we studied the scaling properties of ω as a function of time.

The above results describe the dependence of the average collision number on $t\varepsilon^2$, α_r, and ε. The appropriate scaling variables of the average collision number are α_r and $\varepsilon^x(t\varepsilon^2)$. We will show that x is related to the critical exponents. Near the transition from unlimited to limited energy growth we suppose that the average collision number obeys the relation

$$N(\alpha_r,\varepsilon^x(t\varepsilon^2)) = lN(l^d\alpha_r,l^e\varepsilon^x(t\varepsilon^2)). \tag{37}$$

Choosing $l=\alpha_r^{-1/d}$, the above expression becomes

$$N(\alpha_r,\varepsilon^x(t\varepsilon^2)) = \alpha_r^{-1/d}N_1(\alpha_r^{-e/d}\varepsilon^x(t\varepsilon^2)). \tag{38}$$

Therefore, we rewrite the above expression as

$$N(\alpha_r,\varepsilon^x(t\varepsilon^2)) \propto \alpha_r^{-1/d}(\alpha_r^{-e/d}\varepsilon^x(t\varepsilon^2))^{\xi}. \tag{39}$$

In the initial growth regime of N we have that $\xi=\xi_1$. In this limit the quantity N does not depend on α_r. From Eq. (34) we find $-1/d-e\xi_1/d=0$ and $x\xi_1=\eta_1$. In the second growth regime we have that $\xi=\xi_2$ and from Eq. (35) we obtain $-1/d-e\xi_2/d=\zeta$ and $x\xi_2=\eta_2$.

The expression (38) furnishes the crossover $t_z\varepsilon^2\propto\alpha_r^{e/d}\varepsilon^{-x}$. Thus we have from Eq. (36) that $z_1=-x$ and $z_2=e/d$. Regarding both the $t\varepsilon^2\ll t_z\varepsilon^2$ and $t\varepsilon^2\gg t_z\varepsilon^2$ regimes, we have from the above relations that $x=\eta_1/\xi_1=\eta_2/\xi_2=-z_1\approx-3$, $d=-1/(\xi_1z_2)=-1/(\zeta+\xi_2z_2)\approx1$, and $e=-1/\xi_1=(\zeta-\xi_1z_2)/(\xi_1\xi_2z_2)\approx-3/2$.

Finally, Fig. 16 shows that by performing the variable transformations $N\to N/l$ and $t\varepsilon^2\to l^et\varepsilon^2\varepsilon^x$, $l=\alpha_r^{-1/d}$, we obtain the collapse of the average collision number into a single and universal curve. This result confirms that the scaling hypotheses are correct.

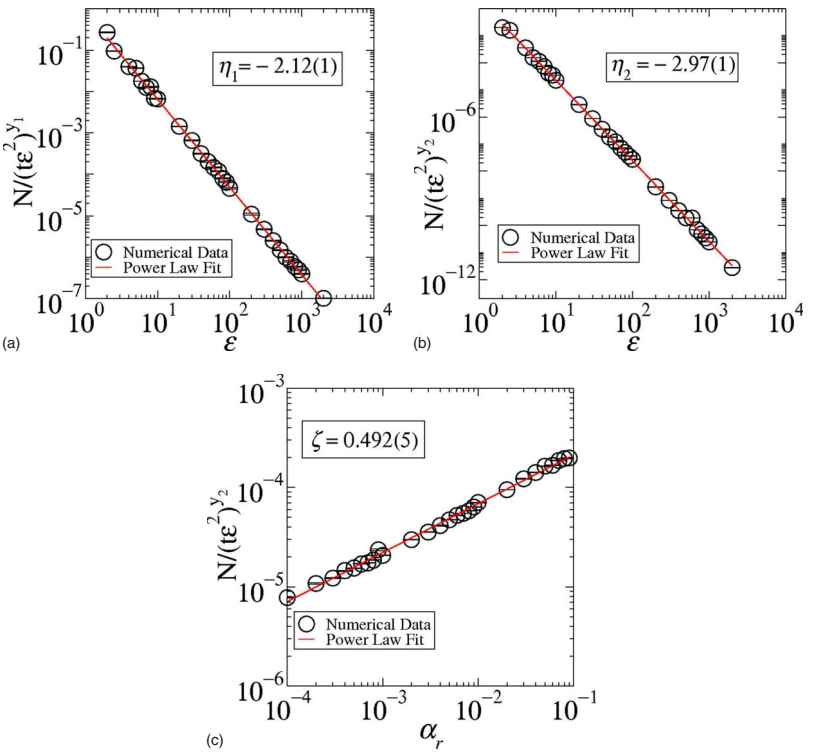

FIG. 15. (Color online) (a) A least-squares fit to the numerical data in an $N/(t\varepsilon^2)^{\xi_1}$ vs ε plot furnishes $\eta_1=-2.12\pm0.01$. (b) The best fit to the data in an $N/(t\varepsilon^2)^{\xi_2}$ vs ε plot furnishes $\eta_2=-2.97\pm0.01$. (c) The best fit to the numerical data in an $N/(t\varepsilon^2)^{\xi_2}$ vs α_r plot furnishes $\zeta=0.492\pm0.005$.

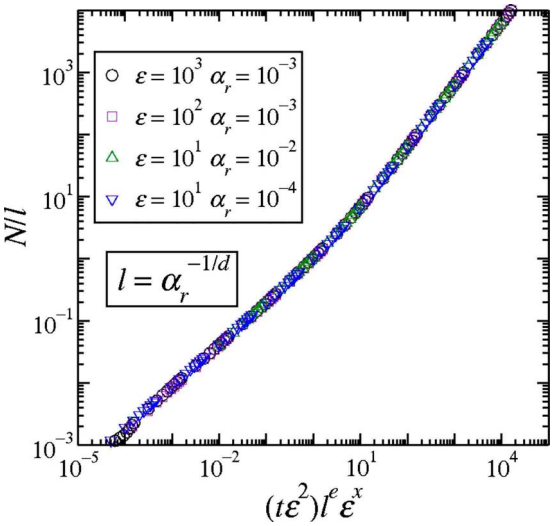

FIG. 16. (Color online) After appropriate variable transformations the average collision number collapses into a universal curve.

IV. DISCUSSIONS AND CONCLUSIONS

In Sec. II we showed that ω grows with the variable $n\varepsilon^2$ according to the relation $\omega(n) \propto (n\varepsilon^2)^\beta$, with $\beta \approx 1/2$. In the analysis of the variable $t\varepsilon^2$ (Sec. III A) we obtained that ω grows according to $\omega(t) \propto (t\varepsilon^2)^\beta$, with $\beta \approx 1/3$.

As we discussed in Sec. III B the average collision number curves present two growth regimes, as we see in Fig. 14. The initial growth regime of N depends on time according to $N \propto (t\varepsilon^2)^{\xi_1}$. Thus we rewrite this expression as $t\varepsilon^2 \propto N^{1/\xi_1}$. We replace this result in Eq. (29), writing $\omega \propto N^{\beta/\xi_1}$. Because $\xi_1 \approx 2/3$ and $\beta \approx 1/3$ we find, therefore, $\omega \propto N^{1/2}$.

As a short summary, we have studied the bouncer model, considering both the complete and simplified versions. We have described the behavior of the deviation around the average velocity for chaotic orbits using the description in terms of n (number of collisions with the moving wall) and time t. Despite the difference of having multiple collisions with the moving wall before leaving the collision zone in the complete version, a situation that is forbidden to happen in the simplified model, the critical exponents obtained are the same for both complete and simplified versions. The description in terms of time also allows a characterization in terms of a scaling analysis. However, since a particle with low energy can suffer many more collisions with the moving wall as compared to a high-energy particle in the same interval of time, the critical exponents obtained are different from those obtained for the description in terms of n. Therefore, both descriptions allow the characterization of the phase transition from limited to unlimited energy growth when the control parameter $\alpha \to 1$.

ACKNOWLEDGMENTS

The authors acknowledge Dr. Amjed A. H. Mohammed for fruitful discussions. We also acknowledge the support from CNPq, FAPESP, and FUNDUNESP, Brazilian agencies.

[1] S. Ulam, in *Proceedings of the Fourth Berkeley Symposium on Mathematical Statistics and Probability*, edited by J. Neyman (University of California Press, Berkeley, 1961), Vol. 3, p. 315.
[2] J. M. Hammerseley, in *Proceedings of the Fourth Berkeley Symposium on Mathematical Statistics and Probability* (Ref. [1]), Vol. 3, p. 79.
[3] A. V. Milovanov and L. M. Zelenyi, Phys. Rev. E **64**, 052101 (2001).
[4] A. Veltri and V. Carbone, Phys. Rev. Lett. **92**, 143901 (2004).
[5] K. Kobayakawa, Y. S. Honda, and T. Samura, Phys. Rev. D **66**, 083004 (2002).
[6] G. Lanzano *et al.*, Phys. Rev. Lett. **83**, 4518 (1999).
[7] F. Saif, I. Bialynicki-Birula, M. Fortunato, and W. P. Schleich, Phys. Rev. A **58**, 4779 (1998).
[8] A. Steane, P. Szriftgiser, P. Desbiolles, and J. Dalibard, Phys. Rev. Lett. **74**, 4972 (1995).
[9] A. Loskutov and A. B. Ryabov, J. Stat. Phys. **108**, 995 (2002).
[10] S. O. Kamphorst and S. P. de Carvalho, Nonlinearity **12**, 1363 (1999).
[11] L. D. Pustylnikov, Trans. Mosc. Math. Soc. **2**, 1 (1978); Theor. Math. Phys. **57**, 1035 (1983).
[12] The bouncer model consists of a classical particle bouncing against a periodically time-varying wall in the presence of a constant gravitational field.
[13] A. Loskutov, A. B. Ryabov, and L. G. Akinshin, J. Phys. A **33**, 7973 (2000).
[14] R. E. de Carvalho, F. C. Sousa, and E. D. Leonel, Phys. Rev. E **73**, 066229 (2006).
[15] A. Y. Loskutov, A. B. Ryabov, and L. G. Akinshin, J. Exp. Theor. Phys. **89**, 966 (1999).
[16] R. Egydio de Carvalho, F. C. de Sousa, and E. D. Leonel, J. Phys. A **39**, 3561 (2006).
[17] F. Lenz, F. K. Diakonos, and P. Schmelcher, Phys. Rev. Lett. **100**, 014103 (2008).
[18] S. O. Kamphorst, E. D. Leonel, and J. K. L. da Silva, J. Phys. A: Math. Theor. **40**, F887 (2007).
[19] R. M. Everson, Physica D **19**, 355 (1986).
[20] G. A. Luna-Acosta, Phys. Rev. A **42**, 7155 (1990).
[21] M. A. Naylor, P. Sanchez, and M. R. Swift, Phys. Rev. E **66**, 057201 (2002).
[22] J. M. Luck and A. Mehta, Phys. Rev. E **48**, 3988 (1993).
[23] A. Mehta and J. M. Luck, Phys. Rev. Lett. **65**, 393 (1990).
[24] P. J. Holmes, J. Sound Vib. **84**, 173 (1982).
[25] T. Vicent and A. I. Mees, Int. J. Bifurcation Chaos Appl. Sci. Eng. **10**, 579 (2000).
[26] A. Kini, T. L. Vincent, and B. Praden, Trans. ASME, Ser. C: J. Heat Transfer **128**, 330 (2006).
[27] A. C. J. Luo and R. P. S. Han, Nonlinear Dyn. **10**, 1 (1996).
[28] A. J. Lichtenberg, M. A. Lieberman, and R. H. Cohen, Physica D **1**, 291 (1980).
[29] E. D. Leonel, J. Phys. A: Math. Theor. **40**, F1077 (2007).
[30] J. K. L. da Silva, D. G. Ladeira, E. D. Leonel, P. V. E. Mc-

Clintock, and S. O. Kamphorst, Braz. J. Phys. **36**, 700 (2006).
[31] E. D. Leonel and P. V. E. McClintock, J. Phys. A **38**, 823 (2005).
[32] E. D. Leonel, P. V. E. McClintock, and J. K. L. da Silva, Phys. Rev. Lett. **93**, 014101 (2004).
[33] A. K. Karlis, P. K. Papachristou, F. K. Diakonos, V. Constantoudis, and P. Schmelcher, Phys. Rev. Lett. **97**, 194102 (2006).
[34] D. G. Ladeira and Jafferson Kamphorst Leal da Silva, Phys. Rev. E **73**, 026201 (2006).
[35] A. K. Karlis, P. K. Papachristou, F. K. Diakonos, V. Constantoudis, and P. Schmelcher, Phys. Rev. E **76**, 016214 (2007).
[36] J.-P. Eckman and D. Ruelle, Rev. Mod. Phys. **57**, 617 (1985).
[37] E. D. Leonel and A. L. P. Livorati, Physica A **387**, 1155 (2008).
[38] The Fermi-Ulam model consists of a classical particle, in the total absence of any external field, confined in and suffering collisions between two walls. One of them is fixed and the other one is periodically moving.
[39] A. J. Lichtenberg and M. A. Lieberman, *Regular and Chaotic Dynamics*, Applied Mathematical Sciences Vol. 38, (Springer-Verlag, New York, 1992).